


Micrometer-Scale Ion Current Rectification at Polyelectrolyte Brush-Modified Micropipets

Xiulan He,^{†,‡} Kailin Zhang,[†] Ting Li,^{†,‡} Yanan Jiang,[†] Ping Yu,^{*,†,‡} and Lanqun Mao^{†,‡} 

[†]Beijing National Laboratory for Molecular Science, Key Laboratory of Analytical Chemistry for Living Biosystems, Institute of Chemistry, the Chinese Academy of Sciences, Beijing 100190, China

[‡]University of Chinese Academy of Sciences, Beijing 100049, China

 Supporting Information

ABSTRACT: Here we report for the first time that ion current rectification (ICR) can be observed at the micrometer scale in symmetric electrolyte solution with polyimidazolium brush (PimB)-modified micropipets, which we call micrometer-scale ion current rectification (MICR). To qualitatively understand MICR, a three-layer model including a charged layer, an electrical double layer, and a bulk layer is proposed, which could also be extended to understanding ICR at the nanoscale. Based on this model, we propose that when charges in the charged layer are comparable with those in the bulk layer, ICR would occur regardless of whether the electrical double layers are overlapped. Finite element simulations based on the solution of Poisson and Nernst–Planck equations and in situ confocal laser scanning microscopy results qualitatively validate the experimental observations and the proposed three-layer model. Moreover, possible factors influencing MICR, including the length of PimB, electrolyte concentration, and the radius of the pipet, are investigated and discussed. This study successfully extends ICR to the micrometer scale and thus opens a new door to the development of ICR-based devices by taking advantage of ease-in-manipulation and designable surface chemistry of micropipets.

Ion current rectification (ICR) is a physical phenomenon by which ion current in one direction is greater than that in the other, which can be attributed to uneven transport of anions and cations across a biological or nanostructured channel.^{1–3} ICR by solid-state nanopores and nanochannels has recently attracted much attention because of its potential applications in fluidic logic circuits (i.e., iontronics),^{4–6} nanoionics,⁷ and biosensors.^{8–10} Hence, ICR has been investigated in various nanosystems,^{1–19} including nanopipets,^{11,12} conical polymer pores,^{3,4} conical glass pores,^{13–16} SiN nanochannels,¹⁷ and protein channels.^{1,8} However, ICR has so far been observed mostly at nanometer scales, and it is difficult to achieve when the pore diameter is 10 times larger than the Debye length.²⁰ There are quite limited reports on observing ICR at a micrometer scale mainly by introducing more asymmetric factors.^{21–23} For example, Mayer et al. demonstrated a method to generate ICR at micropipets with diameters ranging from 10 nm to 2.2 μm by using asymmetric electrolyte solution, and assigned the main driving force for ICR to the electroosmotic

flow.²¹ Shao et al. and Zhu et al. observed ICR at a micrometer scale by using PEI-coated or biconical pipets.^{22,23} To the best of our knowledge, no efforts have been made on polyelectrolyte brush-modified micropores to realize ICR, although polyelectrolyte brushes have been used to tailor the inner surface of nanopores in literature.^{24–28}

Herein, we find that micrometer-scale ICR (MICR) can be easily obtained at polyimidazolium brush (PimB)-modified micropipets. PimB-modified micropipets were controllably fabricated by surface-initiated atom transfer radical polymerization (SI-ATRP, Supporting Information S1) at their inner surfaces. As shown in Figure 1A, a standard linear current–

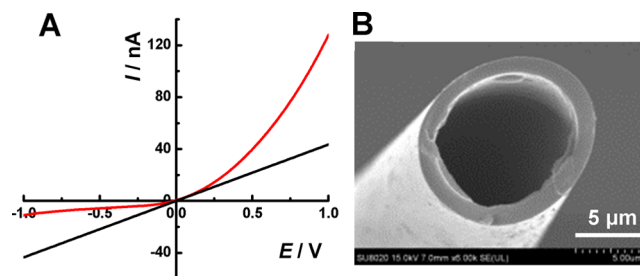


Figure 1. (A) I – V curves obtained at a bare micropipet (black curve) and PimB-modified micropipet (red curve) in 10 mM KCl solution. The voltage sweep was in the direction from -1 V to $+1$ V. Scan rate, 50 mV/s. (B) SEM image of a PimB-modified micropipet. Scale bar, 5 μm .

voltage curve consistent with previous reports was obtained at bare pipets (i.e., without PimB modification) of 5 μm in radius (black curve) in 10 mM KCl solution, because the pipet radius was much larger than the thickness of the electrical double layer (ca. 3 nm).^{11,29} Interestingly, a typical nonlinear current–voltage curve (that is, the current in positive potential window was far greater than that in negative potential window) was observed in 10 mM KCl solution after the micropipet was modified with PimB (red curve). The scanning electron microscopy (SEM) image shows the orifice of a PimB-modified pipet with a radius of ca. 5 μm (Figure 1B), essentially demonstrating that inner modification with PimB did not change the pipet diameter. In other words, MICR occurred at the PimB-modified micropipet even though the thickness of the

Received: November 11, 2016

Published: January 18, 2017

electric double layer (i.e., $\kappa^{-1} \approx 3$ nm) was much smaller than the radius (i.e., $\alpha \approx 5$ μm) of the pipet (i.e., $\kappa\alpha \approx 1670$).

To investigate the influence of polyelectrolyte swelling in salt solution on MICR, we prepared PimB-modified silica nanoparticles (SiNPs) and characterized the size of as-prepared PimB-modified particles by SEM in a dried state and dynamic light scattering (DLS) in 10 mM KCl. The difference in the size of PimB-modified SiNPs obtained from SEM imaging (i.e., 186 ± 4 nm) and DLS (i.e., 216 ± 4.84 nm) indicates a ca. 30 nm swelling of the polyelectrolyte in 10 mM KCl (Supporting Information S2, Figure S1A,B),³⁰ which was negligible as compared to the pipet radius, further excluding an overlap of electrical double layers in Figure 1A (red curve). Although previous studies have pointed out that a complete overlap of the double layers is not necessary for ICR,^{20,31,32} the occurrence of ICR at such a large $\kappa\alpha$ value has never been observed for a polyelectrolyte brush-modified channel. To confirm this phenomenon, we fabricated the micropipets in different radii—150 nm, 1 μm , and 10 μm —and found that all pipets showed nonlinear current–voltage (I – V) curves (i.e., MICR) (Supporting Information S3, Figure S2).

The occurrence of MICR was considered to originate from the charge of the polyelectrolyte brush, which was then confirmed by the reversed rectification when the negatively charged polyelectrolyte brush was used to modify the pipet (Supporting Information S4, Figure S3). The main difference between nanoscale ICR and MICR appeared to be associated with the difference in the charge density on the inner surface of the pipets: for nanoscale ICR with glasses or polymers, the surface charge density varied from 1 mC/m^2 to several tens of mC/m^2 , while for MICR in our case, the space charge density in the polyelectrolyte layer was estimated to be 4.3×10^7 C/m^3 .

To qualitatively understand MICR, a three-layer model was proposed, as shown in Figure 2. As we all know, the ionic

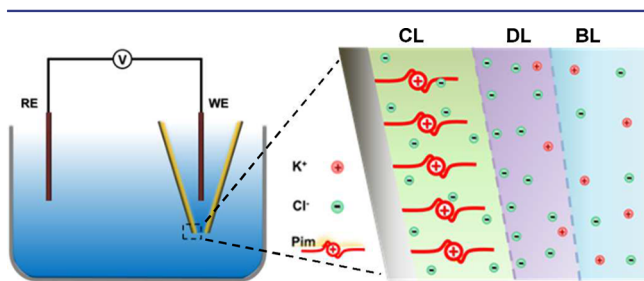


Figure 2. Schematic illustration of the proposed three-layer model including a charged layer (CL), a double layer (DL), and a bulk layer (BL).

current through a nanochannel or nanopore is dominated by the ionic concentration near the orifice of the pore at a specific potential.^{15,21} There are three kinds of ions contributing to the total ionic current in the present system: the counterions in PimB (defined as charged layer (CL), green zone in Figure 2, right panel), the ions in the electrolyte diffusion layer (defined as the electrical double layer (DL), pink zone in Figure 2, right panel), and the ions in the middle of the pipet, which are unaffected by the surface electrostatic field (defined as the bulk layer (BL), blue zone in Figure 2, right panel). For a nanopore, the cross-sectional area at the opening can be used to estimate the possibility of ICR, as demonstrated by Bard et al.¹¹ However, both simulation and experiments show that the distribution of ions at the pore opening is nonuniform.^{31–33}

Therefore, we proposed to use the total amounts of ions (i.e., quantity of electrical charges) to predict the occurrence of ICR. Governed by the rule of electric neutrality, the total amount of ions in CL and DL when no potential was applied across the pipet could be estimated on the basis of the surface charge of PimB obtained from the following equation:

$$Q_s = \rho N z e f \pi L (2\alpha + L \tan \theta) \quad (1)$$

where ρ is the inner surface grafting density, N is the degree of polymerization, z is the charge number of the monomer, e is the elementary charge, f is the dissociation of PimB, L is the effective length of the pipet, α is the orifice radius, and θ is the half cone angle of the pipet. The surface charge (Q_s) was calculated to be 1.65×10^{-7} C under the present conditions (Supporting Information S5).

For the BL presumably under no influence of electrostatic forces, the total amount of ions could be estimated from the electrolyte concentration by using the following equation:

$$Q_b = 2V_b C_b N_A e \quad (2)$$

where V_b is the volume of the BL, C_b is the electrolyte concentration, N_A is the Avogadro constant, and e is the elementary charge. The total quantity of charges carried by ions was calculated to be 1.38×10^{-7} C when the electrolyte concentration of KCl was 0.01 M (Supporting Information S6).

When a potential was applied across the pipet, ions in the CL and the DL were controlled by both electrostatic force and bias electric field force, while ions in the BL were controlled only by the bias electric field. The ion concentration in the BL would be the same in both positive and negative potentials, considering the same mobility of K^+ and Cl^- . Therefore, the current difference at positive and negative potentials was dominated by free counterions in the CL and the DL (i.e., Q_s). When $Q_s \ll Q_b$, no ICR occurred, and a linear I – V curve was obtained (Figure 1, black curve). After the micropipet was modified with PimB, Q_s and Q_b determined from the equations above became comparable, and MICR was observed in terms of the nonlinear I – V curve shown in Figure 1 (red curve). Taking these together, we proposed that when Q_s is larger than or comparable with Q_b , ICR would take place.

Based on this three-layer model (Figure 2), the current at a specific potential can be reduced to calculate the resistance in each part at steady state. Note that, in the present system, we only considered the CL and the BL to simplify the calculation, since we believe that the DL bears the same variation trend of resistance with the CL. By dividing the resistance of each zone into massive infinitesimal parallel-plate resistance, the current was given by the following equation (for derivation see Supporting Information S7):

$$I = 2U / \sum_{\alpha}^{\alpha+L \tan \theta} \frac{\alpha_{n+1} - \alpha_n}{C_{b,n} \alpha_n^2} + 2U / \sum_{\alpha}^{\alpha+L \tan \theta} \frac{\alpha_{n+1} - \alpha_n}{C_{s,n} \alpha_n (1 + \kappa^{-1})} \quad (3)$$

where $C_{s,n}$ and $C_{b,n}$ are the concentration of counterions in the CL and the concentration of the bulk solution in a specific infinitesimal unit (n), respectively.

When the positive potential was applied, C_s increased due to the accumulation of ions (i.e., Cl^-) at the CL and DL by ion movement from the high charge density area to the low charge density area, resulting in the high conductive state (Figure 3A,

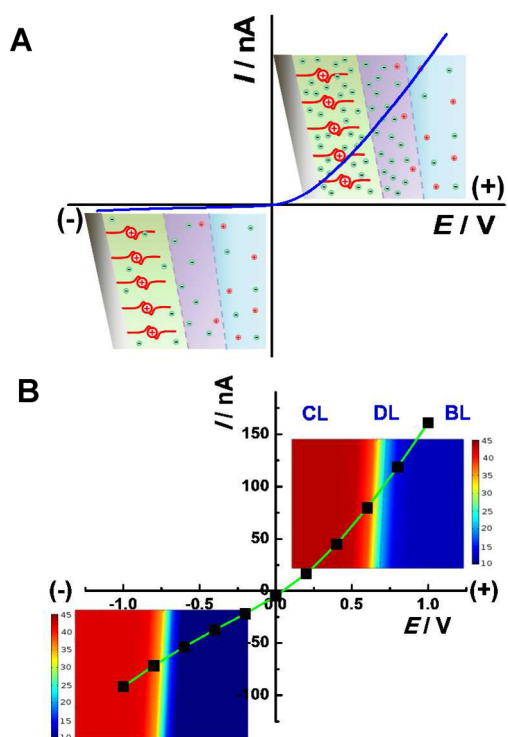


Figure 3. (A) Schematic illustration of the ion distribution at negative and positive potentials based on the three-layer model proposed in Figure 2. (B) Simulated I - V curve of a $5\text{-}\mu\text{m}$ -radius pore with a 300-nm -length polyelectrolyte brush layer. The space charge density was $4 \times 10^6 \text{ C/m}^3$. Inset, the total ion distribution at the junction of the polyelectrolyte brush layer and the bulk layer.

inset in positive potential). Conversely, C_s decreased due to the depletion of ions in both the CL and DL when the negative potential was applied, and the resulting low conductive state was observed (Figure 3A, inset in negative potential; for derivation see Supporting Information S8).

To validate the proposed model, finite element simulation was carried out based on solution of the Poisson–Nernst–Planck equation for symmetric KCl solution (10 mM) within a positively charged polyelectrolyte-modified micropipet (Supporting Information S9). As shown in Figure 3B, the numerically simulated I - V response for the micropipet with a radius of $5 \mu\text{m}$ mainly supports our experimental observation that rectification occurred upon inner surface modification by polyelectrolytes. Moreover, the ion concentration in the middle part was almost the same as that in the bulk solution (Figure S5). Close inspection of the vicinity of the inner wall suggests three kinds of layers, corresponding to the CL, the DL, and the BL, as proposed in our model. To validate the role of Q_s , the space charge density of the polyelectrolyte layer (ρ_c) and the length of the polyelectrolyte brush (L_c) were investigated (Figures S6 and S7). With increasing ρ_c and L_c (i.e., Q_s), the rectification ratio (RR) was increased. When ρ_c was very small, that is, $Q_s \ll Q_b$, no obvious rectification occurred (Figure S6). When Q_s was comparable with or larger than Q_b , rectification occurred. Furthermore, in situ confocal laser scanning microscopy results experimentally highlighted the role of the polyelectrolyte brush in anionic enrichment (Supporting Information S10, Figure S8, and movies 1–6).

To experimentally explore the effect of the total surface charge on MICR, we prepared a series of PimB-modified

micropipets with different polymerization times. For ATRP reaction, the length of the polymer brush was mainly controlled by polymerization time when other conditions were kept the same according to previous reports.^{34,35} As shown in Figure 4A,

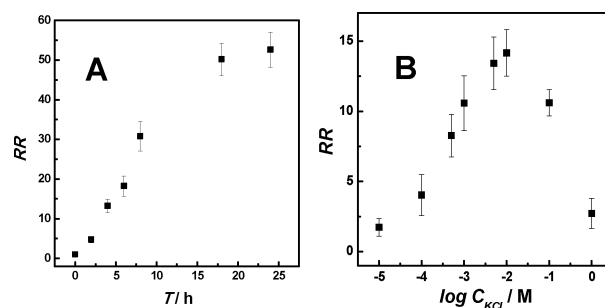


Figure 4. (A) Dependence of the rectification ratio (RR) on polymerization time of PimB. (B) Dependence of RR on KCl concentration for the PimB-modified micropipets.

with increasing polymerization time, the length of the polymer brush (i.e., the total surface charge) increased, resulting in an increase of RR (i.e., the current ratio at the opposite voltage) at pipets with the same radius. When the polymerization time was long enough so that the monomer concentration in solution became the rate-limiting factor, the length of the polymer brush stopped increasing as time prolonged, and RR leveled off to yield a plateau in Figure 4A, which was consistent with the results on the SiNPs surface (Figure S1C) and previously reported results.³⁶ This result experimentally demonstrated the dominance of MICR by the total surface charge (Q_s), further validating the proposed three-layer model.

The dependence of RR on the electrolyte concentration was also investigated at the PimB-modified micropipet. As shown in Figure 4B, a peak-shaped curve was drawn between RR and the logarithmic concentration of KCl, and the largest RR was obtained at 10 mM KCl solution for the $5\text{-}\mu\text{m}$ -radius micropipet. This is a result of a synergistic combination of various factors. One is the thickness of the DL, which is also the dominant factor in nanoscale ICR,³ and another is the length of the polymer brush that shows a complex change with the electrolyte concentration.³⁶ Moreover, the dissociation degree of the polymer brush at different salt concentrations would also affect RR.³⁷ Different from ICR at a nanopore, MICR could be clearly observed at relatively high electrolyte concentrations up to 1 M KCl (i.e., $\kappa\lambda \approx 16700$) (Figure 4B), suggesting that microdevices based on MICR may be used in high-salt systems (e.g., serum or brain microdialysate). Moreover, the MICR at the PimB-modified micropipets was almost pH-independent (Supporting Information S11, Figure S9).

In summary, we have observed ICR at the polyelectrolyte brush-modified micropipet, essentially extending the knowledge of ICR from the nanoscale to the microscale (MICR). Compared with ICR at the nanoscale, MICR bears the following unique properties: (1) the thickness of the electric double layer is much smaller than the orifice radius; (2) MICR can be obtained in high-salt solutions; (3) MICR can be modulated by tuning the polyelectrolyte length and, as such, the type of polyelectrolytes; (4) the diversity of polyelectrolyte essentially endows MICR with more designability; and (5) the relatively large size of the micropipets makes MICR-based devices easier to handle, which is particularly useful for practical

applications, such as in vivo sensing, and will thus pave a new avenue for nanoionics and iontronics.

■ ASSOCIATED CONTENT

Supporting Information

The Supporting Information is available free of charge on the ACS Publications website at DOI: 10.1021/jacs.6b11696.

Experimental details, Scheme S1, and Figures S1–S9 (PDF)

Movie 1, real-time concentration change of PimB-modified micropipet in 10 mM KCl containing 1 μ M 5-carboxyfluorescein at an applied potential of -3 V (AVI)

Movie 2, real-time concentration change of PimB-modified micropipet in 10 mM KCl containing 1 μ M 5-carboxyfluorescein at an applied potential of $+3$ V (AVI)

Movie 3, real-time concentration change of bare micropipet in 10 mM KCl containing 1 μ M 5-carboxyfluorescein at an applied potential of -3 V (AVI)

Movie 4, real-time concentration change of bare micropipet in 10 mM KCl containing 1 μ M 5-carboxyfluorescein at an applied potential of $+3$ V (AVI)

Movie 5, real-time concentration change of PimB-modified micropipet in 10 mM KCl containing 1 μ M Rhodamine B at an applied potential of -3 V (AVI)

Movie 6, real-time concentration change of PimB-modified micropipet in 10 mM KCl containing 1 μ M Rhodamine B at an applied potential of $+3$ V (AVI)

■ AUTHOR INFORMATION

Corresponding Author

*yuping@iccas.ac.cn

ORCID

Lanqun Mao: 0000-0001-8286-9321

Notes

The authors declare no competing financial interest.

■ ACKNOWLEDGMENTS

This work is financially supported by NSF of China (Grant Nos. 21475138 and 21322503 for P.Y. and 21621062, 21435007, and 21210007 for L.M.), the National Basic Research Program of China (2013CB933704 and 2016YFA0200104), and the Chinese Academy of Sciences. The authors thank Dr. Long Luo at The University of Texas at Austin for helpful discussions about the simulation.

■ REFERENCES

- (1) Caterina, M. J.; Schumacher, M. A.; Tominaga, M.; Rosen; Levine, J. D.; Julius, D. *Nature* **1997**, *389*, 816–824.
- (2) Rollings, R. C.; Kuan, A. T.; Golovchenko, J. A. *Nat. Commun.* **2016**, *7*, 11408.
- (3) Siwy, Z. S. *Adv. Funct. Mater.* **2006**, *16*, 735–746.
- (4) Siwy, Z. S.; Howorka, S. *Chem. Soc. Rev.* **2010**, *39*, 1115–1132.
- (5) Ali, M.; Mafe, S.; Ramirez, P.; Neumann, R.; Ensinger, W. *Langmuir* **2009**, *25*, 11993–11997.
- (6) Chun, H.; Chung, T. D. *Annu. Rev. Anal. Chem.* **2015**, *8*, 441–462.
- (7) Cheng, L.; Guo, L. J. *Chem. Soc. Rev.* **2010**, *39*, 923–938.
- (8) Clapham, D. E. *Nature* **2003**, *426*, 517–524.
- (9) Howorka, S.; Siwy, Z. *Chem. Soc. Rev.* **2009**, *38*, 2360–2384.

(10) Umehara, S.; Karhanek, M.; Davis, R. W.; Pourmand, N. *Proc. Natl. Acad. Sci. U. S. A.* **2009**, *106*, 4611–4616.

(11) Wei, C.; Bard, A. J.; Feldberg, S. W. *Anal. Chem.* **1997**, *69*, 4627–4633.

(12) Sa, N.; Lan, W.; Shi, W.; Baker, L. A. *ACS Nano* **2013**, *7*, 11272–11282.

(13) Momotenko, D.; Girault, H. H. *J. Am. Chem. Soc.* **2011**, *133*, 14496–14499.

(14) Guerrette, J. P.; Zhang, B. *J. Am. Chem. Soc.* **2010**, *132*, 17088–17091.

(15) Lan, W.; Holden, D. A.; White, H. S. *J. Am. Chem. Soc.* **2011**, *133*, 13300–13303.

(16) Zhang, B.; Galusha, J.; Shiozawa, P. G.; Wang, G.; Bergren, A. J.; Jones, R. M.; White, R. J.; Ervin, E. N.; Cauley, C. C.; White, H. S. *Anal. Chem.* **2007**, *79*, 4778–4787.

(17) Chen, P.; Mitsui, T.; Farmer, D. B.; Golovchenko, J.; Gordon, R. G.; Branton, D. *Nano Lett.* **2004**, *4*, 1333–1337.

(18) Jin, P.; Mukaibo, H.; Horne, L. P.; Bishop, G. W.; Martin, C. R. *J. Am. Chem. Soc.* **2010**, *132*, 2118–2119.

(19) Macrae, M. X.; Blake, S.; Mayer, M.; Yang, J. J. *Am. Chem. Soc.* **2010**, *132*, 1766–1767.

(20) Kovarik, M. L.; Zhou, K.; Jacobson, S. C. *J. Phys. Chem. B* **2009**, *113*, 15960–15966.

(21) Yusko, E. C.; An, R.; Mayer, M. *ACS Nano* **2010**, *4*, 477–487.

(22) Liu, S.; Dong, Y.; Zhao, W.; Xie, X.; Ji, T.; Yin, X.; Liu, Y.; Liang, Z.; Momotenko, D.; Liang, D.; Girault, H. H.; Shao, Y. *Anal. Chem.* **2012**, *84*, 5565–5573.

(23) Chang, F.; Chen, C.; Xie, X.; Chen, L.; Li, M.; Zhu, Z. *Chem. Commun.* **2015**, *51*, 15316–15319.

(24) Yameen, B.; Ali, M.; Neumann, R.; Ensinger, W.; Knoll, W.; Azzaroni, O. *J. Am. Chem. Soc.* **2009**, *131*, 2070–2071.

(25) Tagliazucchi, M.; Rabin, Y.; Szleifer, I. *J. Am. Chem. Soc.* **2011**, *133*, 17753–17763.

(26) Zeng, Z.; Ai, Y.; Qian, S. *Phys. Chem. Chem. Phys.* **2014**, *16*, 2465–2474.

(27) Buchsbaum, S. F.; Nguyen, G.; Howorka, S.; Siwy, Z. S. *J. Am. Chem. Soc.* **2014**, *136*, 9902–9905.

(28) de Groot, G. W.; Santonicola, M. G.; Sugihara, K.; Zambelli, T.; Reimhult, E.; Vörös, J.; Vancso, G. J. *ACS Appl. Mater. Interfaces* **2013**, *5*, 1400–1407.

(29) Bard, A. J.; Faulkner, L. R. *Electrochemical Methods Fundamentals and Applications*; John Wiley & Sons: New York, 2001.

(30) Guo, X.; Ballauff, M. *Langmuir* **2000**, *16*, 8719–8726.

(31) Kubeil, C.; Bund, A. *J. Phys. Chem. C* **2011**, *115*, 7866–7873.

(32) White, H. S.; Bund, A. *Langmuir* **2008**, *24*, 2212–2218.

(33) Momotenko, D.; Cortés-Salazar, F.; Josserand, J.; Liu, S.; Shao, Y.; Girault, H. H. *Phys. Chem. Chem. Phys.* **2011**, *13*, 5430–5440.

(34) Ma, H.; Hyun, J.; Stiller, P.; Chilkoti, A. *Adv. Mater.* **2004**, *16*, 338–341.

(35) He, X.; Yang, W.; Pei, X. *Macromolecules* **2008**, *41*, 4615–4621.

(36) Fan, X.; Lin, L.; Dalsin, J. L.; Messersmith, P. B. *J. Am. Chem. Soc.* **2005**, *127*, 15843–15847.

(37) Biessalski, M.; Johannsmann, D.; Rühle, J. *J. Chem. Phys.* **2002**, *117*, 4988–4994.